Optimal Control of H-Mode Tokamak Plasma Temperature based on Pontryagin's Principle

S. Jmal * **M. Tacchi-Bénard** * **E. Witrant** *

* *CNRS, GIPSA-lab, Univ. Grenoble Alpes, 38000 Grenoble, France (e-mail: {slim.jmal, matteo.tacchi, emmanuel.witrant}@gipsa-lab.fr).*

Abstract: This paper studies the decay of an objective functional using a new control technique within Pontryagin's framework. Convergence analysis is carried out on the infinite-dimensional space of Tokamak plasma dynamical state as described by weakly decoupled nonlinear partial differential equations. An adjoint-based optimal control is derived to minimize the deviation from a predefined dynamical trajectory leading to the desired target state at stationary regime, by turning Pontryagin's transversality conditions into a continuum of horizons. A feedback controller is proposed to steer the system efficiently in real-time, as opposed to an open-loop controller resulting from the classical Pontryagin's setting. An algorithm synthesizing the constraint-free optimal controller is used for profile tracking based on experimental data.

Keywords: Thermonuclear fusion, nonlinear PDEs, H-mode Tokamak, Pontryagin's principle.

1. INTRODUCTION

Controlling electronic temperature of fusion plasma inside Tokamaks is crucial for enhancing their performance and achieving breakeven for future commercial viability. High-confinement modes (H-mode) are particularly characterized by higher energy at the plasma center, leading to significantly improved confinement times as Keilhacker (1987) showed. Maintaining a stable temperature profile in this regime is critical to prevent instabilities while ensuring efficient heating and transport control.

Different strategies have been explored for controlling plasma profiles. Early works by Moreau et al. (2008) focused on linearized models using singular perturbation theory to separate time scales and control the magnetic and kinetic profiles. Other approaches like that of Moreau et al. (2013); Witrant et al. (2007) relied on first-principles models that capture the dominant nonlinear dynamics of the plasma. To account for the distributed nature of plasma transport, Felici (2011) among others used spatial discretization methods for profile control, whereas Boyer et al. (2013); Bribiesca Argomedo et al. (2013) employed infinite-dimensional PDE-based control techniques.

While previous studies, for example those of Mavkov et al. (2017, 2018), have addressed plasma dynamics coupling through model reduction and data-driven approximations, our focus is on nonlinear PDE-based control, specifically within Pontryagin (1962)'s optimal control framework. This provides a systematic way to derive optimal control laws by solving a state-adjoint system of constrained PDEs. Instead of using a single target profile, we introduce the concept of a continuum of horizons, dynamically adapting the reference trajectory over time to improve stability and tracking performance.

Control of parabolic partial differential equations (PDEs) in finite time is a central problem in mathematical control theory, with wide-ranging applications spanning from physics to engineering. Among the major methods for achieving that, Pontryagin Maximum Principle (PMP) has emerged as a fundamental tool, extending beyond the finite-dimensional control of ordinary differential equations (ODEs). Indeed, foundational developments through direct and variational methods were made by Fursikov and Imanuvilov (1996), where they relied on Hilbert spaces for exact and approximate controllability. Further advances concerning optimal control of distributed parameter systems are presented by Li and Yong (1991), offering necessary conditions for control in infinite-dimensional settings.

In the specific case of diffusion-type equations, applying PMP involves the coupling of the state dynamics with its adjoint state equation evolving backwards, corresponding to Lagrange multipliers associated with PDE constraints, as rigorously analyzed by Barbu (1993). For semilinear parabolic systems with distributed or boundary controls, a detailed treatment of necessary optimality conditions and numerical methods was done by Tröltzsch (2010). In addition, the seminal work of Lions (1971) established the abstract infinite-dimensional PMP over Hilbert spaces, providing a foundational framework that continues to influence modern developments, including extensions to sparsity and pointwise control constraints, as discussed by Casas et al. (2012).

More recent developments have been made to enrich the theory of Pontryagin (1962). Time optimal control problems for abstract parabolic systems with perturbations were analyzed by Tucsnak et al. (2016) leveraging PMP, highlighting the sensitivity of optimal trajectories and control structures under parameter variations while providing key insights on the robustness of his formulation.

Furthermore, the work of Aronna et al. (2021) provides a refined PMP-based analysis with second-order optimality conditions for the state-constrained control of semilinear parabolic equations.

Model Predictive Control (MPC) strategies for parabolic PDEs have recently gained parallel attention for their ability to iteratively solve optimal control problems with a receding target, as studied by Dubljevic et al. (2006). Receding Horizon Control (RHC) schemes for nonlinear parabolic PDEs with boundary control inputs, specifically, were examined by Hashimoto et al. (2012). More recently, the stabilizing properties of receding horizon strategies in infinite-dimensional settings, particularly for reaction-diffusion systems, have been analyzed by Ito and Kunisch (2002), where control Lyapunov functionals and terminal costs are incorporated to ensure convergence and stability.

Building on these latter advancements in the foundational theory of Pontryagin (1962), this work proposes a new technique for solving optimal control problems of nonlinear parabolic PDEs, particularly the diffusion equation of Tokamaks' plasma temperature, integrating MPC-like feedback mechanisms by continuously tracking reference target states. While retaining the structure of PMP in infinite-dimensional Hilbert spaces, this strategy blends the more recent techniques from RHC. As it is defined, our approach is particularly suited for scenarios with functional-norm control constraints, and even geometric shape constraints but with further technical adaptations. Mainly, the contributions of this paper are:

- Reformulation of the classical open-loop Pontryagin transversality conditions into a continuum of receding horizons leading up to the desired final target.
- Design of a PMP-based optimal control law in the closed-loop RHC-style including an adaptive calibration of the regularization term.
- Analysis of the controller energy-norm regularity and boundedness respecting power input constraints.
- Implementation of a control algorithm tuned on the H-mode Tore Supra Tokamak, demonstrating an effective trajectory tracking of the plasma temperature.

The paper is structured as follows: Section 2 describes the plasma temperature dynamics and formulates the optimal control problem. Section 3 introduces our Pontryagin-based approach for solving the problem as well as a regularity/boundedness analysis and a convergence analysis. Section 4 presents the algorithm and simulation results. Section 5 concludes with future research directions.

NOMENCLATURE

Symbol [Unit]	**Definition**
$a\ [m]$	minor plasma radius
$R\ [m]$	major plasma radius
$B_\phi\ [T]$	toroidal magnetic field
$T_e\ [eV]$	electron temperature
$n_e\ [m^{-3}]$	electron density
$\chi_e\ [m.s^{-2}]$	electron diffusivity
$P_{\text{OH}}\ [J.s^{-1}.m^{-3}]$	Ohmic power density
$P_{\text{aux}}\ [J.s^{-1}.m^{-3}]$	auxiliary power density
$P_{\text{sink}}\ [J.s^{-1}.m^{-3}]$	power density loss
$x\ [m]$	normalized space variable
$k\ [\emptyset]$	empirical coefficient
$\omega_{E\times B}\ [s^{-1}]$	flow shearing rate
$\gamma_{\text{ITG}}\ [s^{-1}]$	ion temperature growth rate
$s_{\text{thres}}\ [\emptyset]$	magnetic shear threshold
$s\ [\emptyset]$	magnetic shear
$q\ [\emptyset]$	safety factor

2. SYSTEM DESCRIPTION AND CONTROL PROBLEM

2.1 Electron Temperature Dynamics

The evolution of the electron temperature $T_e(x,t)$ is governed by a nonlinear parabolic PDE modeling heat transport in Tokamak plasmas. Under the assumption of toroidal symmetry, the system reduces to the 1D radial diffusion equation studied by Clémençon et al. (2004) in the cylindrical coordinate system with radial variable $x \in [0,1]$ and mixed Dirichlet and Neumann boundary conditions $T_e(1,t) = T_{edge}(t) \approx 0$, $\frac{\partial T_e}{\partial x}(0,t) = 0$, $\forall t \geq 0$

$$\frac{3}{2}\frac{\partial(n_e T_e)}{\partial t} = \frac{1}{a^2}\frac{1}{x}\frac{\partial}{\partial x}\left(x n_e \chi_e \frac{\partial T_e}{\partial x}\right) - P_{sink} + P_{sources} \quad (1)$$

$P_{sources}(x,t)$ includes external heating sources such as Ohmic heating (P_{OH}), Neutral Beam Injection and auxiliary power (P_{aux}) through radio frequency antennas. $P_{sink}(x,t)$ accounts for energy loss mechanisms, such as electron-ion equipartition losses and radiative cooling, which are often neglected in simplified models used by Witrant et al. (2007) Felici (2011).

2.2 Electron Heat Diffusivity Model

Semi-empirical models are employed instead of a fully analytic model for the electron heat diffusivity because of the complexity of plasma heat transport. In this work, we adopt an extended Bohm/gyro-Bohm model developed by Christofides and Chow (2002); Pianroj and Onjun (2012), and later successfully used by Mameche et al. (2019) in transport simulations of H-mode Tokamak plasmas.
The model expresses the electron heat diffusivity as

$$\chi_e = \chi_{ec} \times f_s, \quad \chi_{ec} = (2\chi_{Be} + \chi_{gBe}) f_s. \quad (2)$$

where the classical diffusivity χ_{e_c} is decomposed into Bohm and gyro-Bohm contributions. The latter writes

$$\chi_{gBe} = 5 \times 10^{-6} \sqrt{T_e} \left| \frac{\nabla T_e}{B_{\phi_0}^2} \right| \quad (3)$$

whereas the Bohm diffusivity is expressed as

$$\chi_{Be} = 4 \times 10^{-5} R \left| \frac{\nabla(n_e T_e)}{n_e B_{\phi_0}} \right| q^2 \left(\frac{T_{e,0.8} - T_{e,1}}{T_{e,1}} \right) \quad (4)$$

$T_{e,1}$ (resp $T_{e,0.8}$) represents the electron temperature at $x = 1$ (resp 0.8) and the last ratio represents the phenomena in which the diffusivity decreases when the edge temperature is increased.

The suppression function $f_s(x)$ accounts for the reduced transport due to turbulence stabilization mechanisms

$$f_s(x) = \frac{1}{1 + k \left(\frac{\omega_{E\times B}}{\gamma_{ITG}} \right)^2} \times \frac{1}{\max\left(1, (s - s_{thres})^2\right)} \quad (5)$$

This expression for f_s was derived based on experimental results by Pianroj and Onjun (2012); Sugihara et al. (2001) to ensure that a transport barrier -the pedestal- is properly modelled near the plasma edge.

Decoupling the magnetic effects from the thermal ones for our PDE-based control problem and defining $A = 2/(3a^2)$, we formualte the diffusion coefficient as

$$\chi(x,t) = A\big(B(x) + C(x)\sqrt{T_e(x,t)}\big)\big|\nabla T_e(x,t)\big| \quad (6)$$

where

$$\begin{cases} B(x) = \dfrac{8 \times 10^{-5} R L_{T_e}}{B_{\phi_0}} q^2(x) f_s(x) \\ C(x) = \dfrac{5 \times 10^{-6}}{B_{\phi_0}^2} f_s(x) \end{cases} \quad (7)$$

and the constant L_{T_e} measures the time-averaged temperature gradient from $\big(T_e(0.8) - T_e(1)\big)/T_e(1)$.

Assumption 1. The semi-empirical diffusivity model used here relies on standard control-oriented assumptions, including slow temporal variations of the safety factor profile q compared to the electron temperature and time-averaged representations of density and loss-related coefficients

While these assumptions simplify the transport model, they are consistent with real-time plasma control practice and enable rigorous controller design on a wide range of Tokamak devices. Extensions to more comprehensive transport models, including additional loss mechanisms and faster equilibrium dynamics, are left for future work.

2.3 Optimal Control Problem

We formulate our problem as an optimal control problem in the Pontryagin framework with a continuum of horizons, the time-discretization of which simplifies to the more classical MPC-like receding horizon control. The goal is to reach a desired electronic temperature profile $\bar{T}_e(x)$ for the Tokamak plasma by controlling the net input heating power $u(x,t)$, while ensuring stability of the system. The control law should not only minimize deviations from a dynamically evolving reference trajectory, but also be robust to errors due to inaccuracies in the model described by the dynamical equation

$$\begin{aligned} \frac{\partial T_e}{\partial t} &= \frac{A}{x}\frac{\partial}{\partial x}\left(x\big(B(x) + C(x)\sqrt{T_e}\big)\left(\frac{\partial T_e}{\partial x}\right)^2 \right) + u \\ &\overset{(6)}{=} \frac{1}{x}\frac{\partial}{\partial x}\left(x\chi\frac{\partial T_e}{\partial x}\right) + u \end{aligned} \quad (8)$$

The optimal control problem (OCP) then formulates as the PDE-constrained minimization problem of the distance to a predefined, dynamical trajectory leading to the final-time target at $t_f < \infty$, plus a regularity constraint on the $L^2_x = L^2(xdx)$-norm of the control variable

$$\min_{\substack{T_e \in \mathcal{A} \\ u \in \mathcal{U}}} \left[\int_0^{t_f} \left(\mathcal{J}_1(t, u, T_e[u]) + \frac{\alpha(t)}{2} \|u\|^2_{L^2_x} \right) dt \right] \quad (9)$$

where $\mathcal{A}$ is the set of admissible solutions to equation (8), and $\mathcal{U}$ is the admissible control space, assumed only to be $H^1([0,1])$. The set of intermediate cost functionals $(\mathcal{J}_1(t,\cdot,\cdot))_{t\in[0,t_f]}$ and penalizing terms $(\alpha(t))_{t\in[0,t_f]}$ are detailed in the following sections.

3. A PONTRYAGIN-BASED APPROACH

3.1 Receding Horizon Pontryagin's Principle

Pontryagin's classical setting with one end-point horizon has the inconvenience of providing an open-loop optimal controller independently from the real evolution of the system. It is therefore prone to errors due to numerical instabilities and deviations of the model from reality. Extending it through a smooth continuum of horizons could prevent these problems by providing a feedback optimal controller in a closed-loop with the system. Let the intermediate targets $(\hat{T}_e(\cdot,t))_{t\in[0,t_f]}$ define our receded horizons as an exponential interpolation between the initial state $T_{e,0}(\cdot)$ and the final-time target $\bar{T}_e(\cdot)$

$$\hat{T}_e(x,t) = T_{e,0}(x) + (1 - e^{-\mu t/t_f})\big(\bar{T}_e(x) - T_{e,0}(x)\big) \quad (10)$$

The corresponding intermediate cost functional measuring the distance of the controlled state to that intermediate target is

$$\mathcal{J}_1(t, u, T_e[u]) = \frac{1}{2}\int_0^1 \big(T_e(x,t) - \hat{T}_e(x,t)\big)^2 x dx \quad (11)$$

Given a partition $(t_i)_i$ of the time interval $[0, t_f]$, OCP (9) can be split by linearity into a sum of integrals as below

$$\min_{\substack{T_e \in \mathcal{A} \\ u \in \mathcal{U}}} \Bigg[\sum_{\substack{0 \le \cdot\cdot \le t_i \le \\ t_{i+1} \le \cdot\cdot \le t_f}} \int_{t_i}^{t_{i+1}} \left(\mathcal{J}_1(t, u, T_e[u]) + \frac{\alpha(t)}{2}\|u\|^2_{L^2_x} \right) dt \Bigg]. \quad (12)$$

Riemann sums converging by definition as the width of the summands $\delta t_i := t_{i+1} - t_i \to 0$, we approximate OCP (9)

$$\sum_{\substack{0 \le \cdot\cdot \le t_i \le \\ t_{i+1} \le \cdot\cdot \le t_f}} \delta t_i \min_{\substack{T_e \in \mathcal{A} \\ u \in \mathcal{U}}} \Big[\mathcal{J}_1(t_{i+1}, u, T_e[u]) + \frac{\alpha(t_{i+1})}{2}\|u\|^2_{L^2_x} \Big] \quad (13)$$

This reformulation into subproblems of optimal control brings up the structure of the classical Pontryagin setting in open-loop. Suppose, indeed, that we controlled the system up to a time $[0, t_f[\ni t_i =: t$ along the reference trajectory $\hat{T}_e$. Set the new time horizon $\tau := t_{i+1} \in]t_i, t_f]$

$$\min_{\substack{T_e \in \mathcal{A} \\ u \in \mathcal{U}}} \Big[\mathcal{J}_1(\tau, u, T_e[u]) + \frac{\alpha(\tau)}{2}\|u\|^2_{L^2_x} \Big] \quad (14)$$

Solving this subproblem of optimal control within Pontryagin's framework requires the introduction of an augmented Lagrangian $\mathcal{L}$ via the Lagrange multiplier p:

$$\mathcal{L}(\tau,u,T_e,p) \overset{\text{def}}{=} \mathcal{J}_1(\tau,u,T_e) + \frac{\alpha(\tau)}{2}\int_t^\tau\int_0^1 u(x,t)^2 x\,dx + \Big\langle p, \underbrace{\frac{1}{x}\frac{\partial}{\partial x}\Big(x\chi\frac{\partial T_e}{\partial x}\Big) + u - \frac{\partial T_e}{\partial t}}_{\overset{=0}{(8)}}\Big\rangle_{L^2_x} \tag{15}$$

Separately calculating the PDE-constraint enforcing term

$$\Big\langle p, \frac{1}{x}\frac{\partial}{\partial x}\Big(x\chi\frac{\partial T_e}{\partial x}\Big) + u - \frac{\partial T_e}{\partial t}\Big\rangle_{L^2_x} = \int_t^\tau\int_0^1 pu\,x dx dt$$

$$+ \int_t^\tau \cancel{x\chi p\frac{\partial T_e}{\partial x}\Big|_0^1} dt - \int_t^\tau\int_0^1 \chi\frac{\partial p}{\partial x}\frac{\partial T_e}{\partial x}\,x dx dt \tag{16a}$$

$$+ \int_t^\tau\int_0^1 \frac{\partial p}{\partial t}T_e\,x dx dt - \int_0^1 p(x,\tau)T_e(x,\tau)\,x dx \tag{16b}$$

$$+ \int_0^1 p(x,t)T_e(x,t)\,x dx \tag{16c}$$

where (16a) expands the term $\langle p, \frac{1}{x}\frac{\partial}{\partial x}(x\chi\frac{\partial T_e}{\partial x})\rangle_{L^2_x}$ and (16b)-(16c) expand the term $\langle p, -\frac{\partial T_e}{\partial t}\rangle_{L^2_x}$, both via integration by parts. The boundary term vanishes thanks to the homogeneous Neumann boundary condition $\frac{\partial T_e}{\partial x}(0,\cdot)=0$ and by enforcing Dirichlet boundary condition $p(1,\cdot)=0$ on the costate.

By the homogeneous Dirichlet boundary condition $T_e(1,\cdot)=0$, expression (16a) further simplifies into this form

$$-\int_t^\tau\int_0^1 \chi\frac{\partial p}{\partial x}\frac{\partial T_e}{\partial x}\,x dx dt = -\int_t^\tau \cancel{x\chi\frac{\partial p}{\partial x}T_e\Big|_0^1} dt + \int_t^\tau\int_0^1 \frac{\partial}{\partial x}\Big(x\chi\frac{\partial p}{\partial x}\Big)T_e\,dx dt. \tag{17}$$

Bringing together all the members of equation (15), we get the final expression of the augmented Lagrangian

$$\mathcal{L}(\tau,u,T_e,p) = \int_t^\tau\int_0^1 \Big[pu + \frac{\alpha}{2}u^2\Big]\,x dx dt \tag{18}$$

$$+ \int_0^1 \Big[\frac{1}{2}\big(T_e(x,\tau)-\hat{T}_e(x,\tau)\big)^2 - p(x,\tau)T_e(x,\tau)\Big]\,x dx + \int_t^\tau\int_0^1 \Big[\frac{\partial p}{\partial t} + \frac{1}{x}\frac{\partial}{\partial x}\Big(x\chi\frac{\partial p}{\partial x}\Big)\Big]T_e\,x dx dt + \int_0^1 p(x,t)T_e(x,t)\,x dx$$

Remark 1. The last term is irrelevant to our optimization, since it no longer is a horizon but a given "initial condition" for the optimal control problem on the interval $[t,\tau]$.

At this stage, variations of the Lagrangian will be taken with respect to the triplet state-costate-control (T_e,p,u). For computational simplicity, we assume that the diffusivity is state-independent $\frac{\partial\chi}{\partial T_e}=0$ over the small horizon $[t,\tau]$, since the nonlinear-dependency terms are very small $(B(x),C(x)\ll 1)$. Now we set the Lagrangian stationary with respect to the state

$$0 = \begin{pmatrix}\nabla_{T_e(\cdot,\cdot)}\mathcal{L}\\ \nabla_{T_e(\cdot,\tau)}\mathcal{L}\end{pmatrix} \tag{19}$$

rewrites as the adjoint equation

$$\begin{cases}\dfrac{\partial p}{\partial t} = -\dfrac{1}{x}\dfrac{\partial}{\partial x}\Big(x\chi\dfrac{\partial p}{\partial x}\Big), \quad \text{a.e. on } [0,1]\times[t,\tau]\\ p(x,\tau) = T_e(x,\tau) - \hat{T}_e(x,\tau), \quad \text{a.e. in } [0,1]\end{cases} \tag{20}$$

with Dirichlet boundary condition $p(1,\cdot)=0$ as stated above. Making the Lagrangian stationary with respect to the control yields Pontryagin's optimality condition

$$0 = \nabla_u\mathcal{L} = p + \alpha(\tau)u \tag{21}$$

Injecting (20)-(21) back into the state equation (8) yields the coupled state-costate PDE system on $[0,1]\times[t,\tau]$

$$\begin{cases}\dfrac{\partial T_e}{\partial t} = \dfrac{1}{x}\dfrac{\partial}{\partial x}\Big(x\chi\dfrac{\partial T_e}{\partial x}\Big) - \dfrac{1}{\alpha}p\\ \dfrac{\partial p}{\partial t} = -\dfrac{1}{x}\dfrac{\partial}{\partial x}\Big(x\chi\dfrac{\partial p}{\partial x}\Big)\end{cases} \tag{22}$$

and the following initial-final conditions

$$\begin{cases}T_e(\cdot,t) = T_{e,t}(\cdot)\\ p(\cdot,\tau) = T_e(\cdot,\tau) - \hat{T}_e(\cdot,\tau).\end{cases} \tag{23}$$

Except for the transversality conditions, notice that PMP does not depend on the time horizon choice, so we differentiate the former by making δt arbitrarily small

$$\begin{aligned}\frac{\partial p}{\partial t} &= \lim_{\delta t\to 0}\frac{p(\cdot,t+\delta t)-p(\cdot,t)}{\delta t}\\ &= \lim_{\tau\downarrow t}\frac{\big(T_e(\cdot,\tau)-\hat{T}_e(\cdot,\tau)\big)-\big(T_e(\cdot,t)-\hat{T}_e(\cdot,t)\big)}{\tau-t}\\ &= \frac{\partial T_e}{\partial t} - \frac{\partial\hat{T}_e}{\partial t}.\end{aligned} \tag{24}$$

Substituting (24) back into the state-costate PDEs (22):

$$-\frac{1}{x}\frac{\partial}{\partial x}\Big(x\chi\frac{\partial p}{\partial x}\Big) = \frac{1}{x}\frac{\partial}{\partial x}\Big(x\chi\frac{\partial T_e}{\partial x}\Big) - \frac{1}{\alpha}p - \frac{\partial\hat{T}_e}{\partial t} \tag{25}$$

hence the inverse problem on the adjoint variable p

$$\Big(\frac{1}{\alpha}Id - \frac{1}{x}\frac{\partial}{\partial x}\Big(x\chi\frac{\partial}{\partial x}\Big)\Big)p = \frac{1}{x}\frac{\partial}{\partial x}\Big(x\chi\frac{\partial T_e}{\partial x}\Big) - \frac{\partial\hat{T}_e}{\partial t}. \tag{26}$$

Combining both transversality and stationarity conditions into this quasi-steady solution for the adjoint state, we bypass the difficulty of solving it backward in time as in the original one-end horizon formulation.

We derived a closed-loop optimal controller evolving forward in time alongside the controlled state, guiding the system along a reference trajectory toward the final target and enabling real-time error corrections by feedback.

3.2 Regularity Analysis

In this section, we analyse the regularity of the adjoint state p and thus that of the optimal controller u via Pontryagin's optimality condition (21) in the sense of a certain $W^{m,2}_x = H^m_x$ Sobolev space ($m=1$ in the sequel).

Multiplying (3.1) by p and L^2_x-integrating over the domain

$$\int_0^1 \alpha^{-1}p^2\,x dx - \int_0^1 \frac{1}{x}\frac{\partial}{\partial x}\Big(x\chi\frac{\partial p}{\partial x}\Big)p\,x dx = \int_0^1 \frac{1}{x}\frac{\partial}{\partial x}\Big(x\chi\frac{\partial T_e}{\partial x}\Big)p\,x dx - \int_0^1 \frac{\partial\hat{T}_e}{\partial t}p\,x dx \tag{27}$$

Using Green's identity and the boundary conditions

$$\int_0^1 \alpha^{-1}p^2\,x dx + \int_0^1 \chi\frac{\partial p}{\partial x}^2\,x dx - \cancel{x\chi p\frac{\partial p}{\partial x}\Big|_0^1} = \cancel{x\chi p\frac{\partial T_e}{\partial x}\Big|_0^1} - \int_0^1 \chi\frac{\partial T_e}{\partial x}\frac{\partial p}{\partial x}\,x dx - \int_0^1 \frac{\partial\hat{T}_e}{\partial t}p\,x dx \tag{28}$$

Cauchy-Schwarz inequality applies to the right hand-side

$$\int_0^1 \alpha^{-1}p^2\,xdx + \int_0^1 \chi\frac{\partial p}{\partial x}^2 xdx \leq \tag{29}$$

$$\sqrt{\int_0^1 \chi\frac{\partial T_e}{\partial x}^2 xdx}\sqrt{\int_0^1 \chi\frac{\partial p}{\partial x}^2 xdx} + \tag{30}$$

$$\sqrt{\int_0^1 \frac{\partial \hat{T}_e}{\partial t}^2 xdx}\sqrt{\int_0^1 p^2 xdx}$$

Young's inequality applies to the right hand-side's terms

$$\sqrt{\int_0^1 \chi\frac{\partial T_e}{\partial x}^2 xdx}\sqrt{\int_0^1 \chi\frac{\partial p}{\partial x}^2 xdx} \leq \frac{1}{2}\int_0^1 \chi\frac{\partial T_e}{\partial x}^2 xdx + \frac{1}{2}\int_0^1 \chi\frac{\partial p}{\partial x}^2 xdx \tag{31}$$

along its positive ε-tradeoff Peter-Paul inequality version

$$\sqrt{\int_0^1 \frac{\partial \hat{T}_e}{\partial t}^2 xdx}\sqrt{\int_0^1 p^2 xdx} \leq \frac{1}{4\varepsilon}\int_0^1 \frac{\partial \hat{T}_e}{\partial t}^2 xdx + \varepsilon\int_0^1 p^2 xdx \tag{32}$$

Plugging these new upper bounds back into (29) yields

$$2(\alpha^{-1}-\varepsilon)\|p\|^2_{L^2_x} + \|p\|^2_{\dot{H}^1_{x\chi}} \leq \|T_e\|^2_{\dot{H}^1_{x\chi}} + \frac{1}{2\varepsilon}\|\partial_t\hat{T}_e\|^2_{L^2_x} \tag{33}$$

Maintaining coercivity of the left hand-side's norms requires choosing $0 < \varepsilon \leq \alpha^{-1}$ in the sequel.

Theorem 1. (Weighted Poincaré Inequality). Let $w \in L^\infty(\Omega)$ be a nonnegative function such that $w(x) > 0$ for almost any $x \in \Omega$. Then there exists a constant $C > 0$ such that for all $v \in H^1_w(\Omega)$ verifying $v \equiv 0$ on $\Gamma \subset \partial\Omega$,

$$\int_\Omega w(x)\,v(x)^2\,dx \leq C\int_\Omega w(x)|\nabla v(x)|^2\,dx \tag{34}$$

The optimal Poincaré (1890) constant is $C = \lambda_{1,w}(\Omega)^{-1}$, where $\lambda_{1,w}$ is the first Dirichlet-Laplacian eigenvalue of Ω as characterized by Evans (2022) as the infimum of the weighted Rayleigh quotient $\mathcal{R}_w$ over $H^1_w(\Omega)$

$$\lambda_{1,w}(\Omega) = \inf_{v\in H^1_w(\Omega)}\big[\mathcal{R}_w(v) := \|v\|^2_{\dot{H}^1_w(\Omega)}/\|v\|^2_{L^2_w(\Omega)}\big] \tag{35}$$

and $\|\cdot\|_{\dot{H}^1_w(\Omega)}$ is the w-weighted Sobolev seminorm defined for all $v \in H^1_w(\Omega)$ by $\|v\|^2_{\dot{H}^1_w(\Omega)} = \int_\Omega |\nabla v|^2\,wdx$.

Poincaré inequality holds in this case since the nonnegative weight $w = x\chi \in L^\infty(0,1)$ is almost everywhere positive, as proven by Kufner and Opic (1990)

$$\lambda_{1,x\chi}\|p\|^2_{L^2_{x\chi}} \leq \|p\|^2_{\dot{H}^1_{x\chi}} \tag{36}$$

Conveniently choosing $\varepsilon = \frac{1}{2\alpha}$ for illustrative purposes and combining the inequalities above gives one final estimate

$$\alpha^{-1}\|p\|^2_{L^2_x} + \lambda_{1,x\chi}\|p\|^2_{L^2_{x\chi}} \leq \|T_e\|^2_{\dot{H}^1_{x\chi}} + \alpha\|\partial_t\hat{T}_e\|^2_{L^2_x} \tag{37}$$

which translates into an upper bound for the energy injected via the optimal controller using equation (21)

$$\|u\|^2_{L^2_x} + \lambda_{1,x\chi}\alpha\|u\|^2_{L^2_{x\chi}} \leq \|\partial_t\hat{T}_e\|^2_{L^2_x} + \alpha^{-1}\|T_e\|^2_{\dot{H}^1_{x\chi}} \tag{38}$$

Remark 2. The first term on the right hand-side is finite by construction, since the reference $\hat{T}_e \in H^1((0,t_f),L^2_x)$ was chosen as a regular interpolation so that $\partial_t\hat{T}_e \in L^2_x$, and the second term is proportional to the Dirichlet energy of a controlled diffusion equation in finite time.

From the inequalities above and the finiteness of the upper-bound in inequality (38), it follows that the control variable u and the adjoint state p are both regular in the sense of $H^1_{x\chi}$ Sobolev space and bounded in the L^2_x-energy space. If one aims at sharpening this upper-bound by subtracting the weighted term on the left-hand side from it, one would need quantified error bounds on $\lambda_{1,w}$, as analyzed by Strang et al. (1973) using finite-element discretizations of the Rayleigh quotient $\mathcal{R}_w$ minimizers, following the classical Rayleigh–Ritz principle. With progress in spectral theory of elliptic operators, Henrot (2006) later studied the dependence of $\lambda_{1,w}$ on the domain geometry and weight structure using shape optimization and variational methods. While these refined analyses could provide us with estimates on $\lambda_{1,x\chi}(\Omega)$, their numerical techniques go beyond the scope of the present work and we restrict ourselves to using the positivity of eigenvalues.

As a measure of the total energy injected into the system, we naturally chose the L^2_x-energy norm of the control variable u as roughly bounded in inequality (38)

$$\|u\|_{L^2_x} \leq \sqrt{\|\partial_t\hat{T}_e\|^2_{L^2_x} + \alpha^{-1}\|T_e\|^2_{\dot{H}^1_{x\chi}}} \tag{39}$$

For future refined analysis of the boundedness/regularity, one would need to study the time-evolution of the upper-bound in inequality (38). Here below is one way to do such

Lemma 1.1. (Gradient Flow). The free diffusion equation is the descending gradient flow of the Dirichlet energy.

$$\frac{\partial}{\partial t}\|T_e\|^2_{\dot{H}^1_\chi(\Omega)} = \Big\langle \nabla_{T_e}\|\cdot\|^2_{\dot{H}^1_\chi(\Omega)}, \frac{\partial}{\partial t}T_e\Big\rangle_{L^2(\Omega)} = \Big\langle -\nabla\cdot(\chi\nabla T_e), \nabla\cdot(\chi\nabla T_e)\Big\rangle_{L^2(\Omega)} \leq 0 \tag{40}$$

However, we are dealing with a diffusion equation that is controlled rather than freely evolving, hence the need to add back our control variable u in the last bracket term and perform adequate functional-analytic manipulations on its norm nested in both hand-sides of inequality (38). We settle with reporting results in figure (1) in the sequel.

3.3 Convergence Analysis

We want to prove convergence of the controlled state toward the final target, which is measured by the objective functional

$$\mathcal{J}(t) = \frac{1}{2}\int_0^1 \big(T_e(x,t) - \bar{T}_e(x)\big)^2\,xdx \tag{41}$$

Inserting the intermediate target $\hat{T}_e(\cdot,t)$ between both terms and using the definition of $\hat{T}_e(\cdot,t_f)$

$$\mathcal{J}(t) = \frac{1}{2}\int_0^1 \Big(\big(T_e(x,t) - \hat{T}_e(x,t)\big) + \big(\hat{T}_e(x,t) - \hat{T}_e(x,t_f)\big)\Big)^2 xdx \tag{42}$$

By virtue of the classical arithmetic–geometric inequality

$$\mathcal{J}(t) \leq 2\big(\mathcal{J}_1(t) + \mathcal{J}_2(t)\big) \tag{43}$$

where the two functionals $\mathcal{J}_1$ and $\mathcal{J}_2$ are defined as

$$\begin{cases} \mathcal{J}_1(t) = \frac{1}{2}\int_0^1 \left(T_e(x,t) - \hat{T}_e(x,t)\right)^2 xdx \\ \mathcal{J}_2(t) = \frac{1}{2}\int_0^1 \left(\hat{T}_e(x,t) - \hat{T}_e(x,t_f)\right)^2 xdx \end{cases} \tag{44}$$

Trivially, we see that the second term $\mathcal{J}_2$ is exponentially decaying. Indeed, plugging in the expression of the reference trajectory $\hat{T}_e$ as an exponential interpolation gives

$$\begin{aligned} \mathcal{J}_2(t) &= \frac{1}{2}\int_0^1 \left(\hat{T}_e(x,t) - \hat{T}_e(x,t_f)\right)^2 xdx \\ &= \frac{1}{2}\int_0^1 e^{-2\mu t/t_f}\left(\hat{T}_e(x,0) - \hat{T}_e(x,t_f)\right)^2 xdx \\ &= e^{-2\mu t/t_f}\mathcal{J}_2(0), \quad t \in [0,t_f] \end{aligned} \tag{45}$$

As for the first term $\mathcal{J}_1$, we will show that it remains small thanks to our optimization-based control method, aiming at minimizing the deviation of the controlled state from a given reference trajectory by calibrating in real-time the parameter $\alpha(t)$ based on the evolution of $\mathcal{J}_1(t)$ itself.

More specifically, we want to establish an empirical law governing the penalty term $\alpha(t)$ of the form

$$\dot{\alpha}(t) = \beta(t) \times h(\mathcal{J}_1(t), \dot{\mathcal{J}}_1(t)) \tag{46}$$

where $\beta \in \{-1, 1\}$ is the adjustment sign to compensate overshooting or undershooting a midway-target, defined as

$$\beta(t) = \text{sign}\left(\int_0^1 \left(T_e(x,t) - \hat{T}_e(x,t)\right) xdx\right) \tag{47}$$

and $h \geq 0$ measures the strength of the deviation of $\mathcal{J}_1$ from 0 as detailed below. Intuitively, if $T_e(\cdot,t)$ is above the midway-target $\hat{T}_e(\cdot,t)$ on average , the sign is positive and we amplify the regularity constraint on the control, otherwise we relax it.

To study the effect of α, we intend to calibrate it once using the standard one-horizon Pontryagin setting on the whole time interval $[0,t_f]$ instead of $[t,\tau]$ as developed in Section 3.1. We retrieve the same adjoint equation (20) but on $[0,1]\times[0,t_f]$ alongside Pontryagin's optimality conditions (21) leading to the coupled state-costate PDEs (22) with initial conditions at time $t=0$ and transversality conditions at final time $\tau = t_f$.

Solving the above coupled PDEs using algorithm (1) below for a constant penalty term α gives us the optimal energy $\mathcal{J}^*(\alpha) = \mathcal{J}(u^*, T_e^*, p^*)$ at the optimal triplet (u^*, T_e^*, p^*) solution to PMP with α-regularized Lagrangian $\mathcal{L}$. Doing the same for different values of α allows us to heuristically analyse the variations of $\mathcal{J}^*$ with respect to α around the optimal penalty term $\alpha^* = \arg\min_\alpha \mathcal{J}^*(\alpha)$.

Remark 3. The regularization parameter α is treated as an external tuning parameter rather than an optimization variable within Pontryagin framework to prevent an infeasible fourth PMP equation of the form $0 = \nabla_\alpha \mathcal{L} = \frac{1}{2}\|u\|^2$, which would necessitate regularizating α in turn just as we did for the control u etc. ad infinitum.

Choosing a small penalty term α leads to a solution overshooting the target and vice-versa; a large α leads to a solution undershooting the target. Shang (2013) considered a similar regularization in Biology by supplementing the objective functional with an extra penalty cost to regulate the attack effort of an infectious virus spreading in inhomogeneous epidemic media.

The following quadratic relation best approximates the results obtained from numerical experimentations

$$\mathcal{J}^*(\alpha) = \kappa(\alpha - \alpha^*)^2, \quad \kappa > 0 \tag{48}$$

This empirical relation is valid for a classical one-horizon Pontryagin framework at a fixed time. Extending it to our continuum of horizons setting requires further assumptions on the coefficient κ and the evolving optimal regularizing parameter, that is their time-invariability $\kappa(t) = \kappa$ and $\alpha^*(t) = \alpha^*$

$$\mathcal{J}_1(\alpha(t)) = \kappa(\alpha(t) - \alpha^*)^2 \tag{49}$$

Under these hypothesises, we derive the empirical formula

$$\begin{aligned} \dot{\mathcal{J}}_1(t) = \frac{d}{dt}\mathcal{J}_1(\alpha(t)) &= \frac{\partial \mathcal{J}_1}{\partial \alpha}\cdot\dot{\alpha}(t) \\ &\overset{(49)}{=} 2\kappa(\alpha(t)-\alpha^*)\cdot\dot{\alpha}(t) \\ &\overset{(47)}{=} 2\beta\sqrt{\kappa}\sqrt{\mathcal{J}_1(t)}\cdot\dot{\alpha}(t) \\ \Rightarrow |\dot{\alpha}(t)| = h(\mathcal{J}_1, \dot{\mathcal{J}}_1) &\propto \frac{\dot{\mathcal{J}}_1(t)}{\sqrt{\mathcal{J}_1(t)}} \end{aligned} \tag{50}$$

By including this adaptive feedback mechanism for the regularizing parameter in our algorithm, we complete the synthesis of the optimal control law.

4. CONTROL ALGORITHM IMPLEMENTATION AND SIMULATION RESULTS

4.1 Control Algorithm

The proposed adjoint-based optimal control algorithm, accessible in Subsection 4.3, is specifically tuned to conform with the H-mode configuration of Tore Supra Tokamak for tracking a desired electronic temperature profile $\bar{T}_e$. Simulation results are presented in Subsection 4.2 below. Hereafter is a pseudocode for solving open-loop PMP, which was independently used to fine-tune $\alpha^* = 10$ from experimentation as studied at the end of Subsection 3.3.

Algorithm 1 Forward-Backward Sweep

Input $\alpha, \varepsilon = 10^{-6}, n_{max} = 10^3$
Output u, y, p

```
n ← 0
u_0 ← 0
while ‖u_n − u_{n−1}‖_{L²([0,t_f],L²(Ω))} > ε and n < n_max do
    y_n ← solution to the u_n-controlled state equation
    p_n ← solution to the y_n-conditioned adjoint equation
    u_n ← −α^{−1} ∇_u L(u_n, y_n, p_n)
    n ← n + 1
end while
u ← u_n, y ← y_n, p ← p_n
```

4.2 Simulation Results

All numerical simulations are performed by taking into account the model presented in Subsection 2.2, where the parameters of the heat diffusivity are calibrated on experimental measurements extracted from the Tore Supra shot 36 056 (12/08/2005) obtained with lower hybrid (2.5 MW) and ion cyclotron (5 MW) radio frequency antennas. The free parameters used in Subsection 3.1 are as follows: the final time is set to $t_f = 1$, and the exponentiation parameter in the expression of the reference trajectory is

fixed at $\mu = 5.85$ for an abrupt ramp-up phase at the start of the plasma heating.

Figure 1 reports the time-evolution of the total mean energy inflow needed for the system's control toward an optimal functioning regime as analysed in Subsection 3.2. The grey curve represents the L^2-energy norm of the control, while the blue curve corresponds to the theoretical upper bound derived from functional regularity estimates.

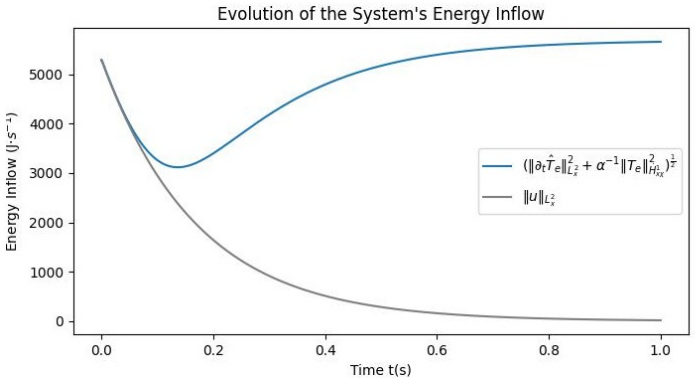

Fig. 1. Boundedness of the Optimal Power Input

From an operational standpoint, maintaining a tight upper bound on the control energy during the ramp-up phase is particularly important for the system's transition toward an optimal confinement regime with minimal expenditure. This energetic efficiency is crucial for setting down power balances given the expected energy release from plasma fusion reactions in such high confinement modes. Despite this upper bound getting loose with time, based on the rough estimate (39), most of the heating energy is rather spent on the fusion plasma ignition during the first phase than on the plasma stabilization.

Figure 2 depicts the space-time evolution of the controlled plasma temperature $T_e(x,t)$ along the prescribed reference trajectory $\hat{T}_c(x,t)$, which was defined as an exponential interpolation connecting the initial state to the experimentally identified stationary target corresponding to the Tore Supra optimal H-mode equilibrium.

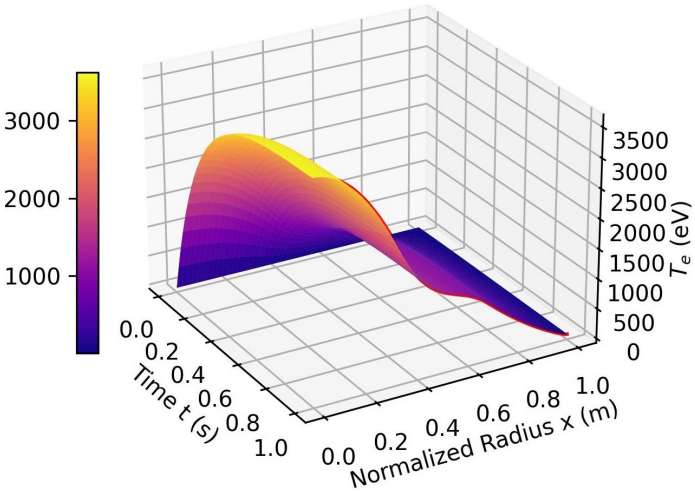

Fig. 2. Controlled Plasma Temperature Evolution

The controlled dynamics remain nearly indistinguishable from the reference trajectory, demonstrating the high fidelity of the control strategy in tracking the desired temperature evolution. Figure 3 further confirms that the controlled temperature profile almost-perfectly matches the final-time target with a discrepancy of $1.01 \cdot 10^{-7}$.

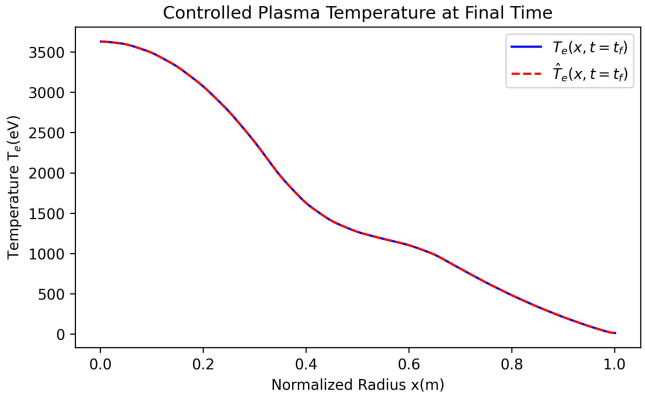

Fig. 3. Controlled Plasma Temperature at Final Time

The space–time distribution of the optimal power input in Figure 4 clearly illustrates the physically expected shape of auxiliary heating in an H-mode Tokamak discharge: an initial, sharp energy deposition localized near the plasma core efficiently triggers the transition to high confinement, while the required power rapidly decreases as the temperature gradient self-sustains through improved confinement. This behavior reproduces the typical pattern observed in high-performance discharges, where feedback actuators operate predominantly during the transient phase.

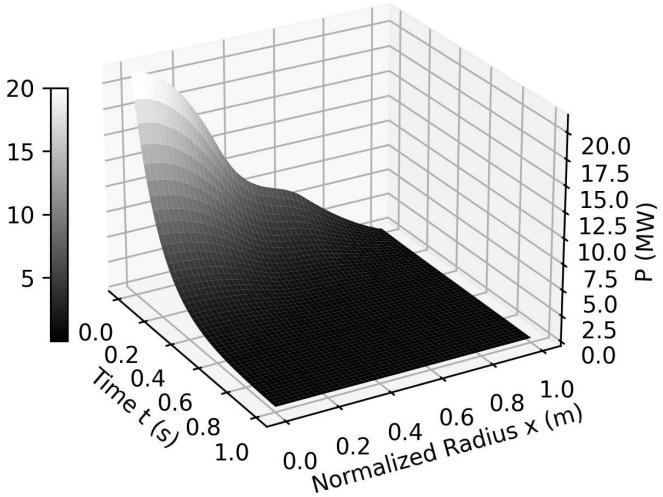

Fig. 4. Optimal Power Input Control Law

Experimentally, the evolution of the optimal controller both reaffirms the energetic feasibility of the control process and validates the estimate derived in Subsection 3.2 regarding the boundedness of the control variable.

As studied in Subsection 3.3, the convergence analysis is further supported by the plots in Figure 5: two almost-overlapping curves; that of the exponentially decaying

reference trajectory in red and that of the main objective functional in blue nearly fitting the former up to a small deviation due to our optimization-based control technique, as rendered more clearly visible on their log-scaled dotted counterparts.

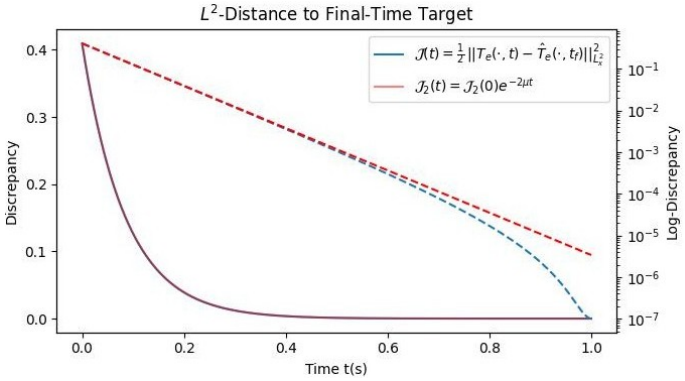

Fig. 5. Convergence of the Objective Functional

The exponential speed of convergence is essentially the same as that imposed on the controlled system through the reference trajectory, until orders of magnitudes below where tiny deviations play out due to control-induced minimization of the first bounding term in inequality (43).

Figure 6 below showcases the evolution of J_1 as a measure of deviation from predefined intermediate targets, topping out at $3.369 \cdot 10^{-6}$ by the end of the control process

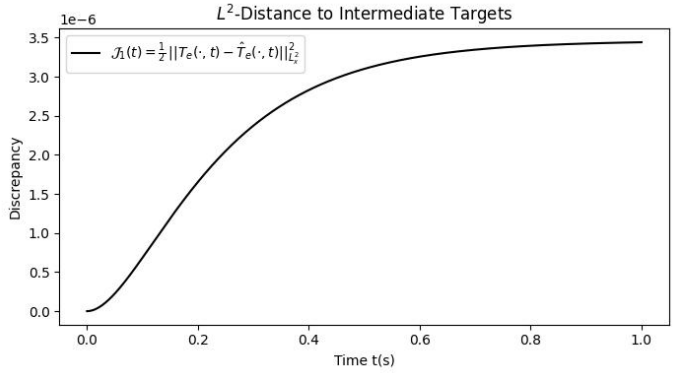

Fig. 6. Tracking the Reference Trajectory

These deviations have been controlled to be as small as possibly allowed by our regularized optimization-based control within Pontryagin's framework, while blending the adaptive law of the regularizating α-parameter into our control algorithm.

4.3 Code Script & Numerical Scheme

The numerical scheme relies on a one-dimensional finite-difference discretization in space and time, with a uniform grid resolution of $N_t = 1000$ time steps and $N_x = 1000$ space points. A mixed implicit–explicit Euler scheme is employed to propagate the controlled state forward in time: diffusion operators are treated implicitly, while nonlinear transport and control-dependent terms are handled explicitly.

At each time step, the control law is computed by solving an inverse problem on the adjoint equation, which is also discretized into the inversion of a linear system obtained from the matrix representation of our differential operators (Laplacian, gradient). The regularization parameter is updated based on the evolution of the tracking functional.

The algorithmic complexity is bilinear $\mathcal{O}(N_t N_x)$ in our best-case scenario of banded matrices, being sparse and tridiagonal as combination of such, and would be linear-cubic $\mathcal{O}(N_t N_x^3)$ in the worst case of dense matrices for higher order schemes. Execution time is about 30 seconds on a standard laptop equipped with a 12th-generation Intel Core i5-1235U processor, using NumPy 1.26.4. version of Python 3.11.

The implemented control algorithm is available at: `https://gitlab.com/slimj-group/SlimJ-project/-/blob/main/Optimal_Control_of_Tokamak_Plasma_Temperature_via_Pontryagin_Receding_Horizon_Principle.ipynb`

5. CONCLUSION

In this work, we introduced an optimal control strategy for fusion plasma dynamics governed by nonlinear PDEs of inhomogeneous diffusion type. The proposed methodology extends the classically open-loop Pontryagin framework into a feedback control mechanism by reformulating the transversality conditions as a continuum of receding intermediate targets, in the spirit of RHC. A closed-loop control law is derived by combining the PMP equations with an adaptive regularization of the control energy norm, ensuring convergence of a performance criterion measuring the deviation of the controlled state from a desired dynamical trajectory. This reformulation enables the systematic conversion of an open-loop optimal control problem into a feedback mechanism, allowing real-time compensation for modeling uncertainties and enhanced robustness with respect to external perturbations. Numerical results were obtained using a control algorithm based on the Bohm/gyro-Bohm transport model and calibrated on the H-mode plasma temperature diffusion of the Tore Supra tokamak. These simulations confirm the effectiveness and energetic efficiency of the proposed strategy for temperature profile tracking.

Beyond its computational simplicity relative to Lyapunov-based designs in infinite-dimensional settings, this work establishes a foundational bridge between optimal control theory and applications in plasma physics. In particular, the continuum-of-horizons interpretation of Pontryagin's transversality conditions offers a flexible paradigm for the control of coupled nonlinear PDEs, as encountered in magnetically confined fusion plasmas, where transport, turbulence, and magnetohydrodynamic phenomena may interact across multiple spatial and temporal scales. Future investigations will incorporate geometric shape constraints and explore real-time implementation on platforms such as TCV's RAPTOR simulator, with a view toward scalability and integration in reactor-scale devices including ITER. For such large-scale systems, more localized dynamics control may be required, as encountered in the field of quantum plasmas, where the evolution is governed by nonlinear Schrödinger-type equations. In this direction, analytical frameworks such as the generalized Riccati equation map-

ping method have been applied in quantum optics Yasin et al. (2024), and could provide a useful foundation for extending the present control strategy to quantum optimal control settings.

ACKNOWLEDGEMENTS

This work has been carried out within the framework of the EUROfusion Consortium, funded by the European Union via the Euratom Research and Training Programme (Grant Agreement No 101052200 - EUROfusion). Views and opinions expressed are however those of the author(s) only and do not necessarily reflect those of the European Union or the European Commission. Neither the European Union nor the European Commission can be held responsible for them. The work of Slim Jmal is supported by the program "Initiatives de Recherche à Grenoble Alpes" through the grant SOS-Fusion.

We thank the anonymous referees for their constructive remarks and for suggesting references that broaden the scope of this contribution, notably by highlighting connections with biological and quantum optimal control applications.

REFERENCES

Aronna, M.S., Bonnans, J.F., and Kröner, A. (2021). State constrained control-affine parabolic problems ii: second order sufficient optimality conditions. *SIAM Journal on Control and Optimization*, 59(2), 1628–1655.

Barbu, V. (1993). *Analysis and Control of Nonlinear Infinite Dimensional Systems*. Academic Press, Boston.

Boyer, M.D., Barton, J., Schuster, E., Luce, T.C., Ferron, J.R., Walker, M.L., Humphreys, D.A., Penaflor, B.G., and Johnson, R.D. (2013). First-principles-driven model-based current profile control for the DIII-D tokamak via lqi optimal control. *Plasma Physics and Controlled Fusion*, 55(10), 105007.

Bribiesca Argomedo, F., Witrant, E., Prieur, C., Brémond, S., Nouailletas, R., and Artaud, J.F. (2013). Lyapunov-based distributed control of the safety-factor profile in a tokamak plasma. *Nuclear Fusion*, 53(3), 033005.

Casas, E., Herzog, R., and Wachsmuth, D. (2012). Sparse solutions to linear pdes in optimal control. *SIAM Journal on Control and Optimization*, 50(4), 1735–1752.

Christofides, P.D. and Chow, J. (2002). Nonlinear and robust control of pde systems: Methods and applications to transport-reaction processes. *Appl. Mech. Rev.*, 55(2), B29–B30.

Clémençon, A., Guivarch, C., Eury, S., Zou, X., and Giruzzi, G. (2004). Analytical solution of the diffusion equation in a cylindrical medium with step-like diffusivity. *Physics of Plasmas*, 11(11), 4998–5009.

Dubljevic, S., El-Farra, N.H., Mhaskar, P., and Christofides, P.D. (2006). Predictive control of parabolic pdes with state and control constraints. *International Journal of Robust and Nonlinear Control: IFAC-Affiliated Journal*, 16(16), 749–772.

Evans, L.C. (2022). *Partial differential equations*, volume 19. American mathematical society.

Felici, F. (2011). *Real-time control of tokamak plasmas: from control of physics to physics-based control*. Ph.D. thesis, EPFL.

Fursikov, A.V. and Imanuvilov, O.Y. (1996). Controllability of evolution equations. *Lecture Notes Series, Seoul National University*, 34.

Hashimoto, T., Yoshioka, Y., and Ohtsuka, T. (2012). Receding horizon control with numerical solution for nonlinear parabolic partial differential equations. *IEEE Transactions on Automatic Control*, 58(3), 725–730.

Henrot, A. (2006). *Extremum problems for eigenvalues of elliptic operators*. Springer.

Ito, K. and Kunisch, K. (2002). Receding horizon optimal control for infinite dimensional systems. *ESAIM: control, optimisation and calculus of variations*, 8, 741–760.

Keilhacker, M. (1987). H-mode confinement in tokamaks. *Plasma Physics and Controlled Fusion*, 29(10A), 1401.

Kufner, A. and Opic, B. (1990). *Hardy-type inequalities*. Longman Scientific & Technical.

Li, X. and Yong, J. (1991). Necessary conditions for optimal control of distributed parameter systems. *SIAM Journal on Control and Optimization*, 29(4), 895–908.

Lions, J.L. (1971). *Optimal control of systems governed by partial differential equations*, volume 170. Springer.

Mameche, H., Witrant, E., and Prieur, C. (2019). Nonlinear pde-based control of the electron temperature in h-mode tokamak plasmas. In *2019 IEEE 58th Conference on Decision and Control (CDC)*, 3227–3232. IEEE.

Mavkov, B., Witrant, E., and Prieur, C. (2017). Distributed control of coupled inhomogeneous diffusion in tokamak plasmas. *IEEE Transactions on Control Systems Technology*, 27(1), 443–450.

Mavkov, B., Witrant, E., Prieur, C., Maljaars, E., Felici, F., Sauter, O., et al. (2018). Experimental validation of a lyapunov-based controller for the plasma safety factor and plasma pressure in the tcv tokamak. *Nuclear Fusion*, 58(5), 056011.

Moreau, D., Mazon, D., Ariola, M., De Tommasi, G., Laborde, L., Piccolo, F., Sartori, F., Tala, T., Zabeo, L., Boboc, A., et al. (2008). A two-time-scale dynamic-model approach for magnetic and kinetic profile control in advanced tokamak scenarios on jet. *Nuclear Fusion*, 48(10), 106001.

Moreau, D., Walker, M.L., Ferron, J.R., Liu, F., Schuster, E., Barton, J.E., Boyer, M.D., Burrell, K.H., Flanagan, S., Gohil, P., et al. (2013). Integrated magnetic and kinetic control of advanced tokamak plasmas on DIII-D based on data-driven models. *Nuclear Fusion*, 53(6), 063020.

Pianroj, Y. and Onjun, T. (2012). Simulations of h-mode plasmas in tokamak using a complete core-edge modeling in the baldur code. *Plasma Science and Technology*, 14(9), 778.

Poincaré, H. (1890). Sur les équations aux dérivées partielles de la physique mathématique. *American Journal of Mathematics*, 211–294.

Pontryagin, L.S. (1962). *Mathematical theory of optimal processes*. Routledge.

Shang, Y. (2013). Modeling epidemic spread with awareness and heterogeneous transmission rates in networks. *Journal of biological physics*, 39(3), 489–500.

Strang, G., Fix, G.J., et al. (1973). *An analysis of the finite element method*, volume 212. Prentice-hall.

Sugihara, M., Igitkhanov, Y., Janeschitz, G., Pacher, G., Pacher, H., Pereverzev, G., and Zolotukhin, O. (2001). Simulation studies on h-mode pedestal behavioru during

type-i elms under various plasma conditions. In *Proceedings of the 28th EPS Conference on Controlled Fusion and Plasma Physics, Funchal, Portugal*, 629–632.

Tröltzsch, F. (2010). *Optimal control of partial differential equations: theory, methods, and applications*, volume 112. American Mathematical Soc.

Tucsnak, M., Wang, G., and Wu, C.T. (2016). Perturbations of time optimal control problems for a class of abstract parabolic systems. *SIAM Journal on Control and Optimization*, 54(6), 2965–2991.

Witrant, E., Joffrin, E., Brémond, S., Giruzzi, G., Mazon, D., Barana, O., and Moreau, P. (2007). A control-oriented model of the current profile in tokamak plasma. *Plasma Physics and Controlled Fusion*, 49(7), 1075.

Yasin, F., Alshehri, M.H., Arshad, M., Shang, Y., and Afzal, Z. (2024). Exploring dynamics of multi-peak and breathers-type solitary wave solutions in generalized higher-order nonlinear schrödinger equation and their optical applications. *Alexandria Engineering Journal*, 105, 402–413.